Accepted Manuscript

Graphene Reinforced Epoxy Adhesive For Fracture Resistance

Zhemin Jia, Xiaoping Feng, Yun Zou

PII: S1359-8368(18)32800-2

DOI: 10.1016/j.compositesb.2018.09.093

Reference: JCOMB 6063

To appear in: *Composites Part B*

Received Date: 27 August 2018

Revised Date: 25 September 2018

Accepted Date: 25 September 2018

Please cite this article as: Jia Z, Feng X, Zou Y, Graphene Reinforced Epoxy Adhesive For Fracture Resistance, *Composites Part B* (2018), doi: https://doi.org/10.1016/j.compositesb.2018.09.093.

Graphene Reinforced Epoxy Adhesive For Fracture Resistance

Zhemin Jia*, Xiaoping Feng, Yun Zou,

School of Environment and Civil Engineering, Jiangnan University, Wuxi, Jiangsu, 214122;

*Corresponding author: jiazhemin123@163.com

Abstract

The fracture resistance of construction adhesive has attracted tremendous interests in the past decades. This paper conducts an experimental study on the mode I fracture resistance of epoxy construction adhesive reinforced with graphene nanoplatelets (GNPs) through double cantilever beam (DCB) specimens. The experimental results show that the mode I fracture toughness of nanocomposites increases compared with the neat epoxy. It is worth noting that the mode I fracture toughness of nanocomposites at a graphene content of only 0.25 wt% exhibit a 5 times enhancement compared with neat epoxy adhesive. When the graphene content continues to increase, the mode I fracture toughness of adhesive decreases as the aggregation of graphene in adhesive. The mechanical behavior of the DCB specimens with different nanocomposites adhesive are predicted using finite elements analysis (FEA). The mode I fracture properties of nanocomposites obtained from the experimental results are used as cohesive zone model parameters in FEA. The prediction agrees very well with the experimental results.

Keywords: Graphene Epoxy; Fracture Resistance; Numerical Analysis

1. Introduction

Epoxy based adhesive joints have been widely used in different applications, including bonding metal components, fiber-reinforced composites (FRP), and concrete structures [1–5]. Epoxy adhesives have shown lots of advantages, such as lightweight, low-cost, and avoiding the use of metal fasteners, which are commonly vulnerable to corrosions [6–11]. To evaluate the quality of adhesives, fracture toughness is an important criterion, because the brittle nature of the epoxy based adhesive joints is the major drawback limiting the service life. In open literatures, people have made a lot of efforts on enhancing the fracture toughness of epoxy based adhesives, but most works still cannot fulfill the requirements in the industries due to the issue of complicated fabrication process, unsatisfactory properties, and relatively high cost.

Recently, polymer based composites have attracted tremendous interest due to their effectiveness in improving the mechanical and other functional properties of epoxy adhesives [12]. Many types of fillers such as metal particles [13, 14] and carbon fillers including carbon nanofibers (CNFs) [15,16], carbon nanotubes (CNTs) [17,18], and graphene [19,20,21], have been studied. For instance, nanofiber was introduced in the epoxy adhesive to improve mechanical performance of the joints. The mechanical performance of the reinforced aluminum joints was investigated by utilizing double cantilever beam (DCB). Mod I fracture toughness of the adhesively bonded joints were found to increase by 97% with addition of nanofiber into epoxy adhesive [22]. Compared with other types of fillers, graphene presents much better performances, resulting from the large aspect ratio, large specific surface area, and

exceptional mechanical strength. Hitherto, graphene/polymer composites have been extensively explored to achieve desired mechanical and other functional properties [23–25].

From the previous works, various graphene fillers such as graphene nanoplatelets (GNPs), reduced graphene oxide (rGO), and three dimensional graphene have been developed [26], and their epoxy based composites possessed excellent mechanical properties. Take GNPs as an example, it has been introduced into a rubber-modified epoxy adhesive in order to simultaneously improve the bulk mechanical properties [27], bulk fracture toughness and single joint lap shear strength of the adhesive. The Young's modulus was observed to increase by 4% and the fracture energy of the bulk adhesive increased by 21 % after adding 0.1 wt.% GNPs. Although the mechanical properties of GNPs/epoxy composites have been extensively studied, the fracture resistance of GNPs/epoxy composites and their applications in construction adhesives are still rarely studied.

Herein, GNPs have been used to reinforce epoxy adhesive. Nanocomposites with different graphene contents, including 0.25 wt%, 0.5 wt%, 0.75 wt% were fabricated. The double cantilever beam (DCB) specimens were used to test mode I critical strain energy release rate of nanocomposites. The variation trend of mode I fracture toughness with the graphene content were obtained. The numerical analysis conducted by ABAQUS was also carried out to simulate DCB specimens with different nanocomposites.

2 Experiment

2.1 Materials

The adhesive used in this paper was manufactured by Kangda Company in Shanghai, a two-component epoxy adhesive which contains component A for epoxy and component B for curing agent. This adhesive has been widely used in the construction area to join fiber reinforced polymer (FRP) to the existing structures. The cure condition of this adhesive is at room temperature (RT) for 72 h according to the manufacturer of adhesive. The GNPs were fabricated by thermally expanding the the graphite intercalated compound (GIC), and the details can be found in our previous works [19, 23]

2.2 Preparation of GNP/epoxy composites

GNPs were dispersed in acetone at a graphene concentration of 2mg/ml, followed by sonication for 6 h in a bath sonicator. Then the GNP/acetone dispersions were mixed with a certain amount of epoxy (component A of the adhesive), depending on the graphene content of the final composites. After that, GNPs and epoxy adhesive were pre-mixed using a magnetic stirrer at 2000 rpm for 3h to evaporate acetone at RT. The temperature of the mixture was subsequently elevated to 100 °C for full evaporation of acetone. After cooling down to RT, curing agent (component B of the adhesive) at a stoichiometric ratio (weight fraction epoxy/ hardener = 3/1) was added into the mixture and mixed using a planetary mixer (ZYMC-180V, ZYE Technology Co., Ltd) at 2000 rpm for 3 min to obtain the final GNP/epoxy composites. Nanocomposites containing three different graphene contents, including 0.25 wt%, 0.5 wt% and 0.75 wt% were prepared.

2.3 Sample fabrication

The mode I fracture toughness of adhesive was investigated using DCB specimens. The specimens were fabricated according to the standard ISO 25217 and the dimensions of the specimens were shown in Fig. 1. Stainless steel was used for the adherends. To control the thickness of adhesive, four 0.1mm-thick spacers, two on each side, were inserted between the adherends before the application of adhesive and the thickness of adhesive was 0.2mm. A sharp pre-crack with the length of 70 mm was fabricated by a 40-μm thick polytef (PTFE) film. The pre-crack was placed in the middle of the spacers to ensure that the pre-crack positions in the mid-plane of adhesive. The spacers were removed after the joints being cured.

As required by the standard ISO 25217, the average thickness and width of the adherends were measured before bonding. The average thickness of the adhesive was obtained by subtracting the respective average thicknesses of the two adherends from the total thickness of the DCB specimen after bonding. Before bonding, the surface of the adherend was first scrubbed with acetone to erase the oil stain and metal oxide on the surface, followed by sanding with 60# sandpaper to increase the roughness of the bonding surface. The sides of the adherends and the surfaces of the spacers were coated with a release agent to avoid excessive adhesive bonding. The adhesive was evenly applied to avoid excessive mixing of air bubbles. The DCB joints were cured at RT for 72 h. After curing, scrape the excess adhesive on the side of joints to complete DCB specimen preparation.

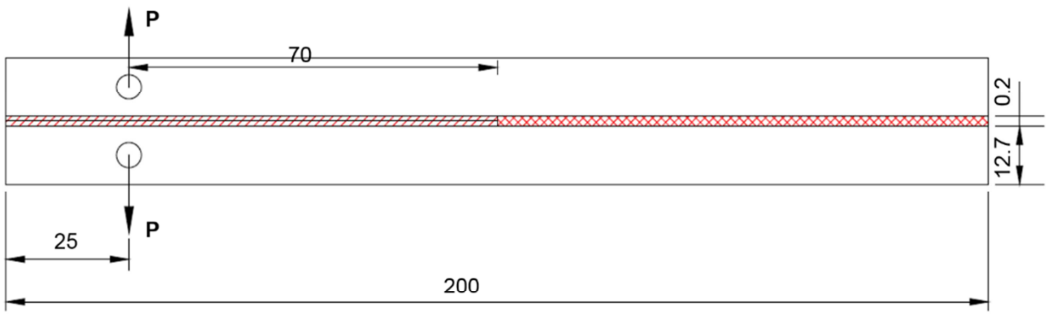

Fig. 1. Illustration of DCB specimen dimensions.

2.4 Test procedure and data analysis

The DCB specimens with GNP/epoxy adhesive and neat epoxy adhesive were tested by an electronic universal testing machine (Zwick 8406) as shown in Fig. 2. To avoid blunted pre-cracks, all the specimens were loaded before the experiment starting until the cracks were extended forward by 2-3 mm on the basis of the pre-cracks. Force-displacement curves were recorded during the experiment. At least four specimens were tested for each material.

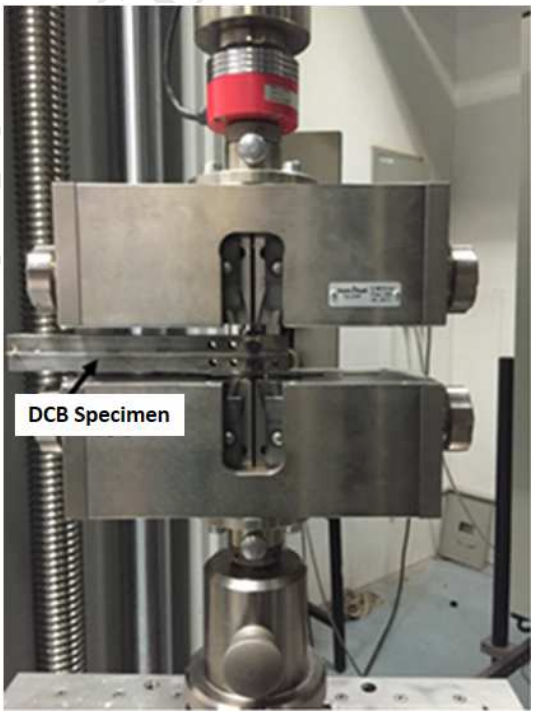

Fig. 2. Experimental set up for DCB specimens

The compliance-based beam method (CBBM) to obtain the mode I fracture toughness of adhesive has been proposed by Moura [28-30]. It does not need the measurement of crack propagation to calculate the mode I fracture toughness of the adhesive. This method has been compared with the traditional methods which need the crack propagation for calculating the mode I fracture toughness of adhesive in the literature and the good consistency is obtained [29, 30]. The mode I fracture toughness of ductile adhesive is calculated by Equation (1-5).

$$G_I = \frac{6P^2}{B^2 h}\left(\frac{2{a_{eq}}^2}{h^2 E_f} + \frac{1}{5G}\right) \tag{1}$$

$$\delta = \frac{8P{a_{eq}}^3}{E_f B h^3} + \frac{12P a_{eq}}{5BhG} \tag{2}$$

$$E_f = \left(C_0 - \frac{12(a_0 + |\Delta|)}{5BhG}\right)^{-1} \frac{8(a_0 + |\Delta|)^3}{Bh^3} \tag{3}$$

$$\Delta = h\sqrt{\frac{E_f}{11G}\left[3 - 2\left(\frac{\Gamma}{1+\Gamma}\right)^2\right]} \tag{4}$$

$$\Gamma = 1.18\frac{\sqrt{E_f E}}{G} \tag{5}$$

where P is the force value; h is the thickness of adherend; B is the width of the specimen; G and E are shear modulus and elastic modulus of the adherend; C_0 is the initial compliance of the specimen and a_0 is the initial crack length which is 70mm in this paper; a_{eq} is the equivalent crack length and the value of a_{eq} can be obtained by solving Equation (2) through Matlab Software; Δ is the rotation correction value of the initial crack; E_f is the flexural modulus of the modified specimen, which takes into account of factors that may affect the P–δ relationship,

such as the stress concentration at the crack tip, changes in the stiffness of the specimen during the experiment etc.

3 Results

3.1 Experimental study on mode I fracture toughness of neat adhesive and GNP/epoxy adhesive

To investigate the effect of graphene content on mode I fracture resistance of epoxy adhesive, tests on DCB specimens with neat epoxy and different content of GNP/epoxy adhesive were carried out. Fig. 3 presents typical force-displacement curves of neat adhesive and GNP/epoxy nanocomposites with three different graphene contents. It can be observed that all three nanocomposites showed higher peak load and maximum displacement than the neat epoxy adhesive, but this improvement was not increased with the increase of GNP content. The nanocomposites containing 0.25 wt% GNP shows the highest peak load and maximum displacement. The R-curves for neat epoxy and nanocomposites were shown in Fig. 4 and the variation trend of mode I critical strain energy release rate with the graphene content was shown in Fig.5 and the specific value of mode I fracture toughness of neat epoxy and nanocomposites with different GNP content were listed in Table 1.

It can be seen from Fig. 5 that the enhancement of mode I fracture toughness was significantly when the GNP content increased to 0.25wt%. The nanocomposite reinforced at a graphene content of 0.25 wt% delivered almost 5 times increase in mode I fracture toughness compared with the neat epoxy, which was the highest improvement among all the materials tested in the paper. However, when the

graphene content continued to increase, the mode I fracture toughness decreased compared with nanocomposites with graphene content of 0.25 wt%. The fracture surfaces of DCB specimens with different content of GNPs were examined by optical microscope, as shown in Fig.6. From Fig.6, the reason to cause the decrease in mode I fracture toughness when the graphene content increased was that the aggregation of GNP in the epoxy adhesive, especially in DCB specimens with the GNPs content of 0.5%.

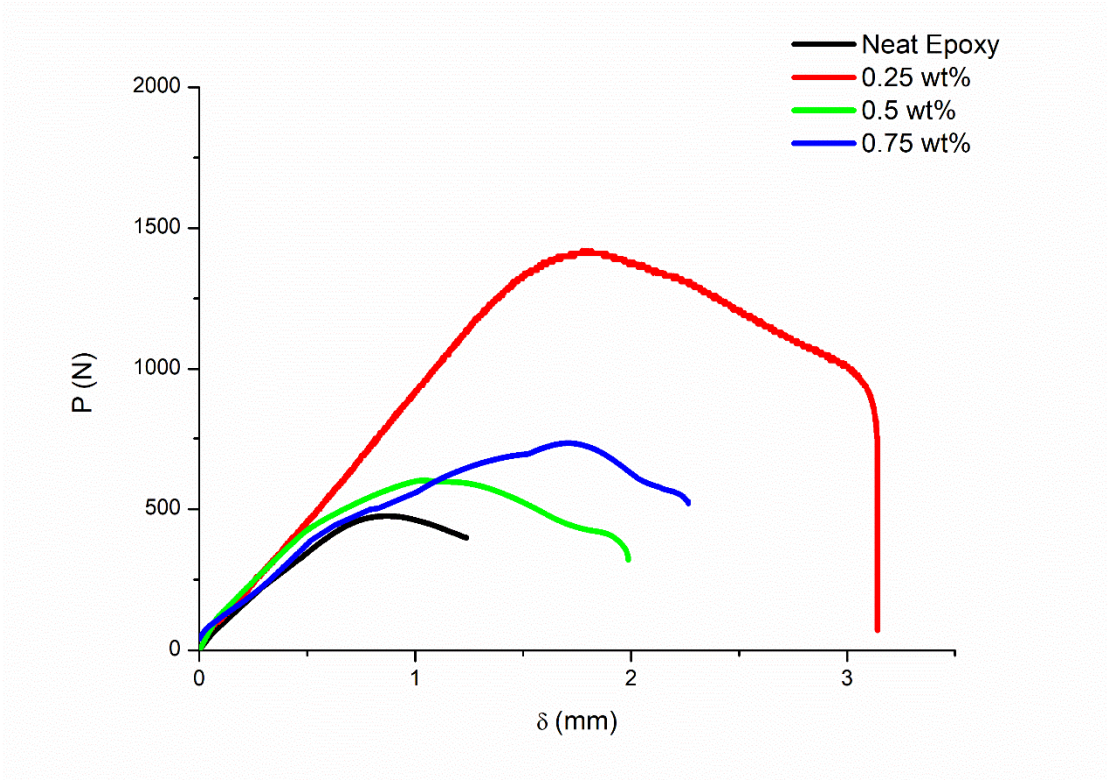

Fig.3 Force-displacement curves of DCB specimens containing neat epoxy and different content of GNP/epoxy nanocomposites.

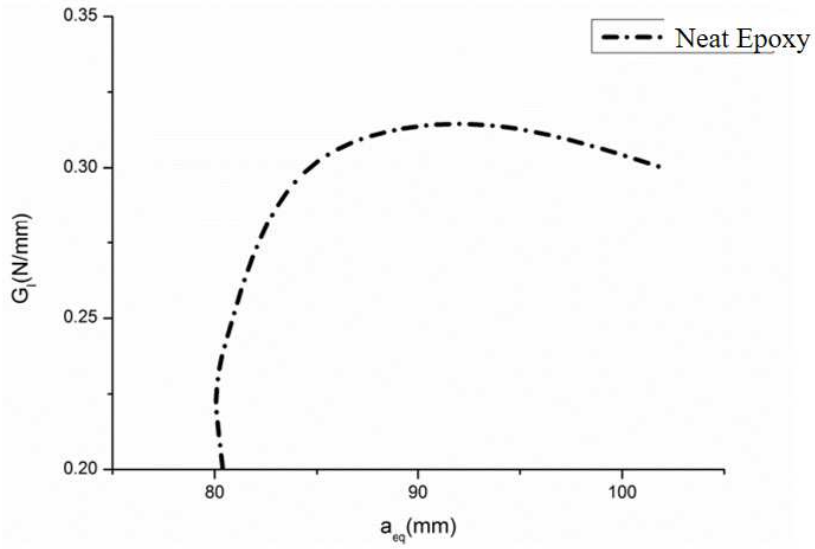

(a) Neat Epoxy

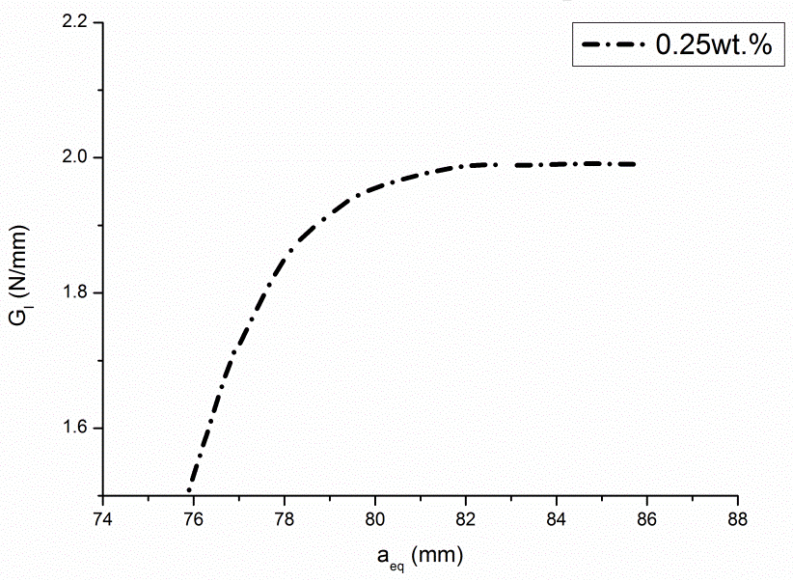

(b) 0.25 wt%

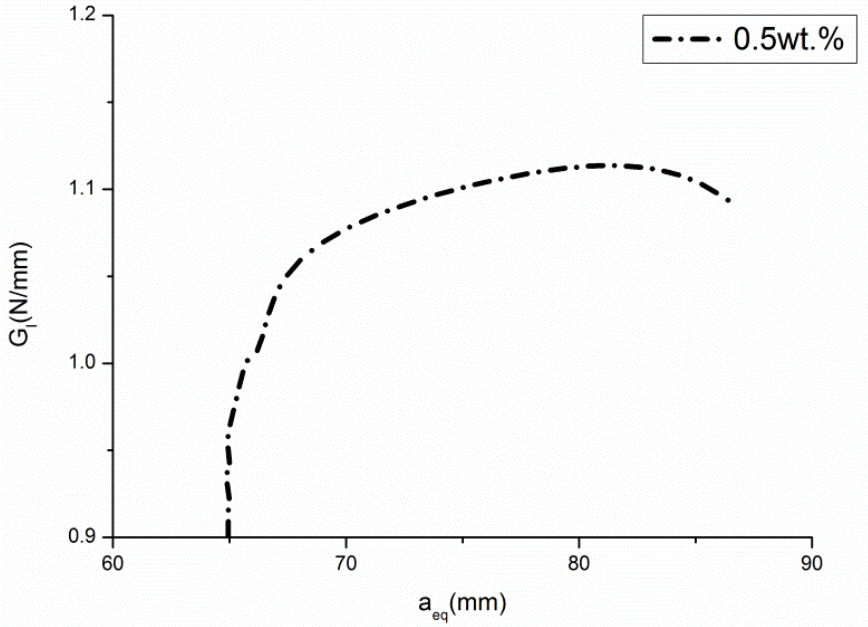

(c) 0.5 wt%

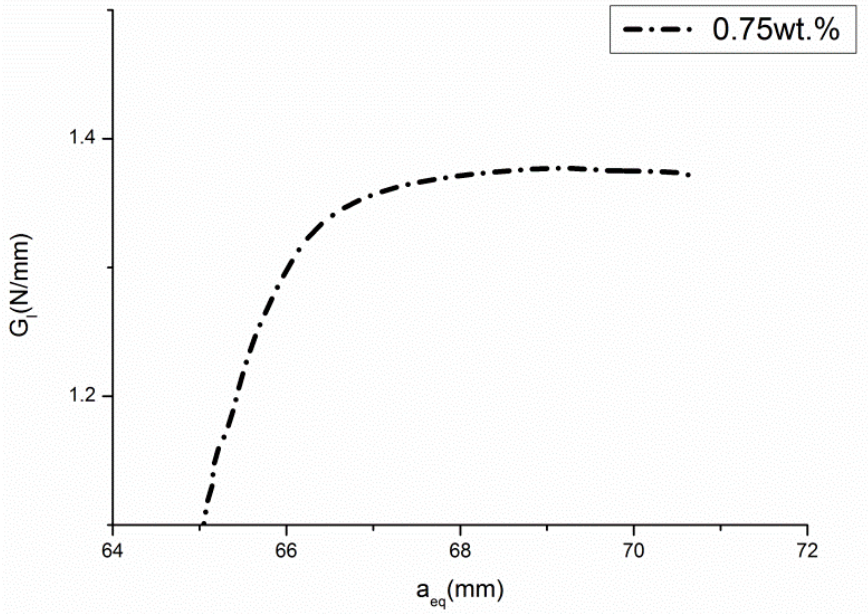

(d) 0.75 wt%

Fig.4 Typical R-curves of DCB specimens containing neat epoxy and different content of GNP/epoxy nanocomposites.

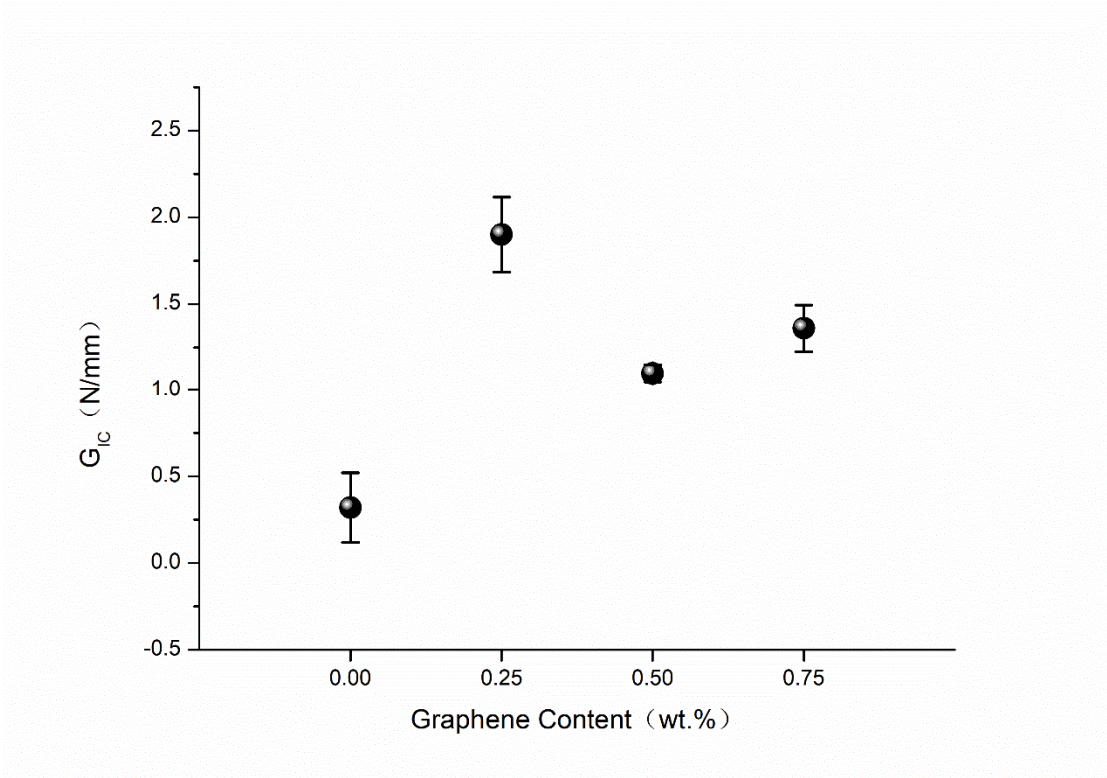

Fig. 5 Mode I fracture toughness of nanocomposites with a function of graphene content

Table 1 Mode I fracture toughness of Neat Epoxy and GNP/Epoxy Nanocomposites.

Graphene Content (wt %)	Mode I fracture toughness (N/mm)	standard deviation (N/mm)
0	0.32	0.201
0.25	1.9	0.216
0.5	1.1	0.049
0.75	1.36	0.134

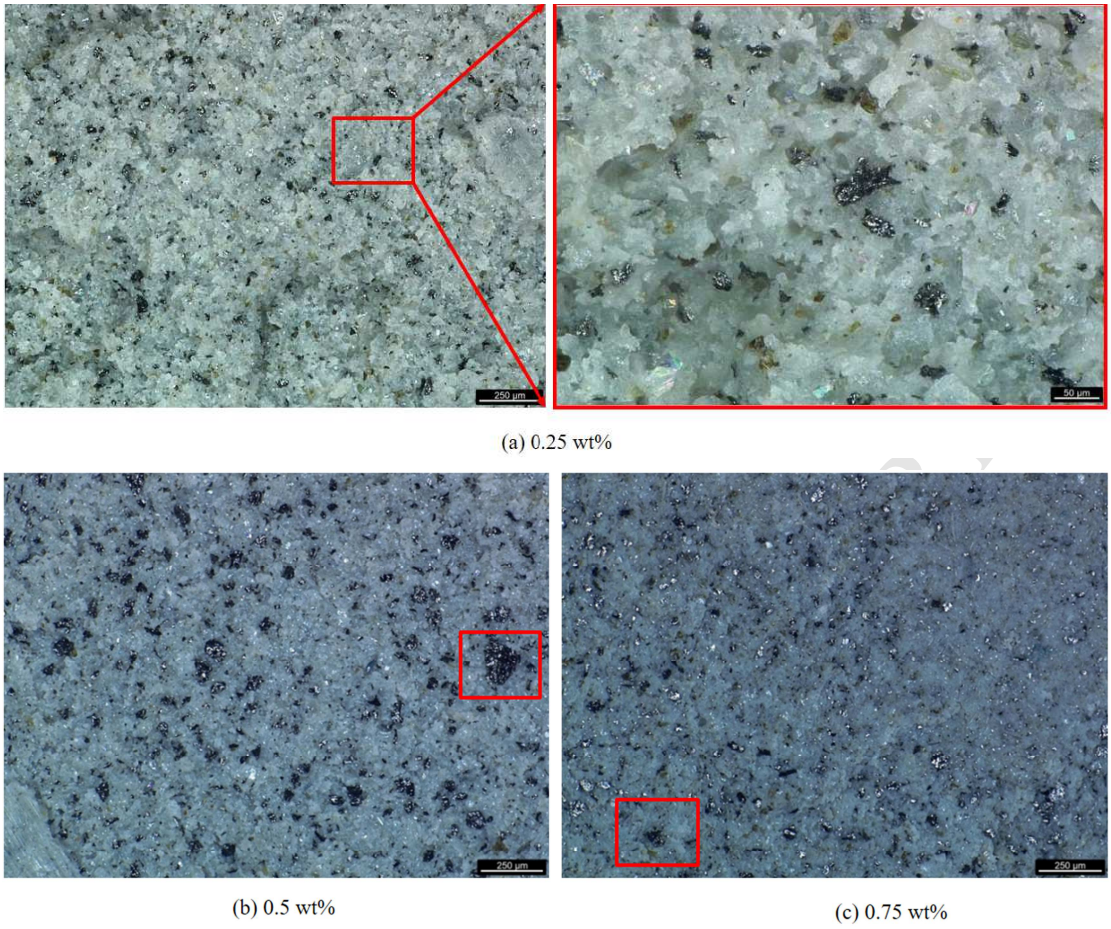

Fig.6 Fracture Surfaces of DCB specimens with different content of GNPs

3.2 Numerical Simulation and Result

DCB specimens containing different nanocomposites were simulated by ABAQUS. The entire analysis was geometrically nonlinear. Meshing diagram of the DCB specimen and the applied boundary conditions were shown in Fig. 7. The plane strain elements (CPE4) with an out-of-plane width of 25 mm were employed for adherend and the adhesive was simulated by two-dimensional 4-node cohesive elements (COH2D4).

The steel adherends were divided into 12 elements in the thickness direction, and the mesh was refined close to the overlap area. The adhesive was divided into one element in the thickness direction due to the instinctive property of cohesive elements.

The boundary conditions were applied according to the experiment, left end of the lower adherend was fixed in the x direction and the y direction and the left end of upper adherend was fixed in the x direction and the experimentally measured maximum displacement was applied in the y direction of the lower adherend.

Elastic-plastic material model was used for adherend steel, as shown in Table 2. The cohesive zone model parameter for neat adhesive and nanocomposites with different GNP content were obtained as follows. The mode I critical strain energy release rate of the adhesive input in the CZM was experimentally tested, cohesive stiffness was obtained by dividing the tensile modulus of the adhesive by adhesive thickness in DCB specimens. The cohesive strength was inputted by the inverse method.

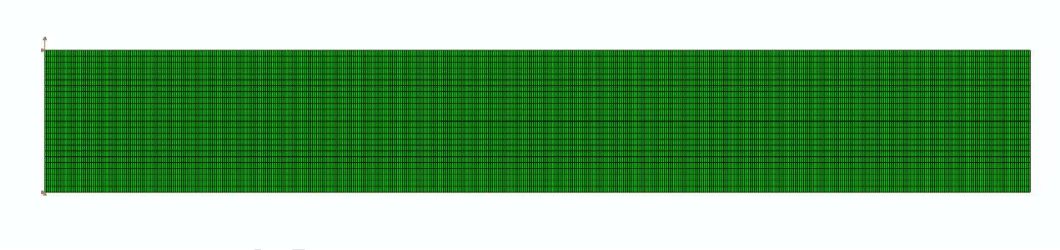

Fig.7 Mesh diagram in DCB specimens

Table 2 List of material properties of the adherends in DCB specimens

Yield stress /MPa	Plastic strain
400	0
420	$2.0e^{-2}$
500	$20.2e^{-2}$
600	$50.0e^{-2}$

Comparisons between the experimental data and FEA results containing nanocomposites were shown in Fig.8. It could be seen that the DCB specimens could be resonably predicted by cohesive zone models.

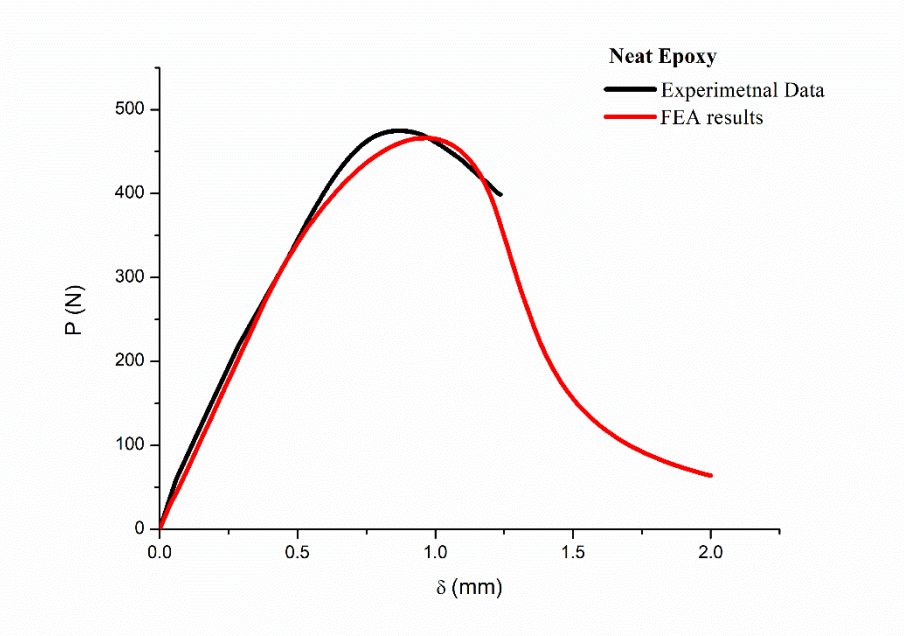

(a) Neat Epoxy

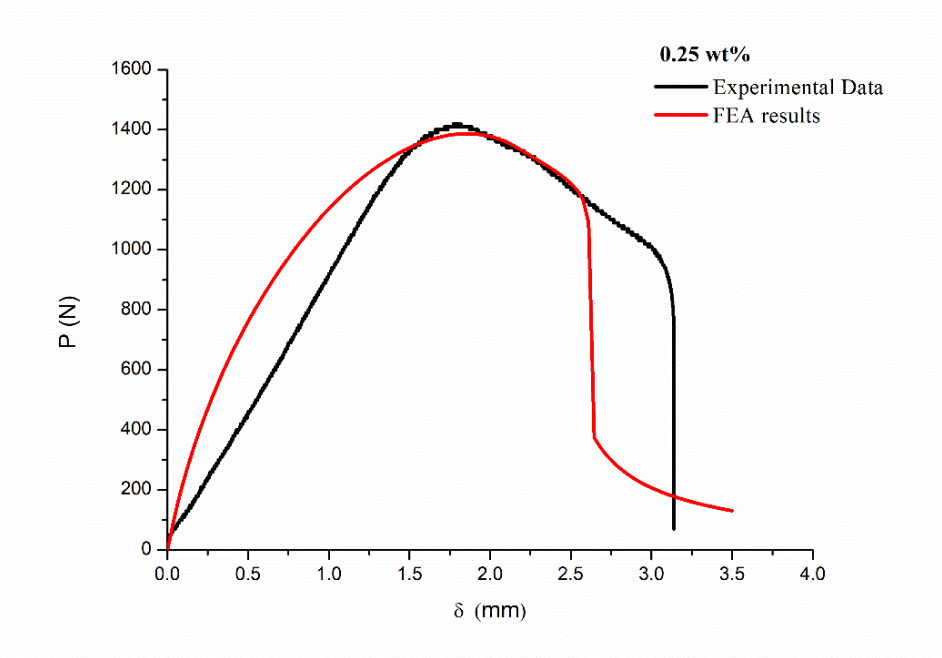

(b) 0.25 wt%

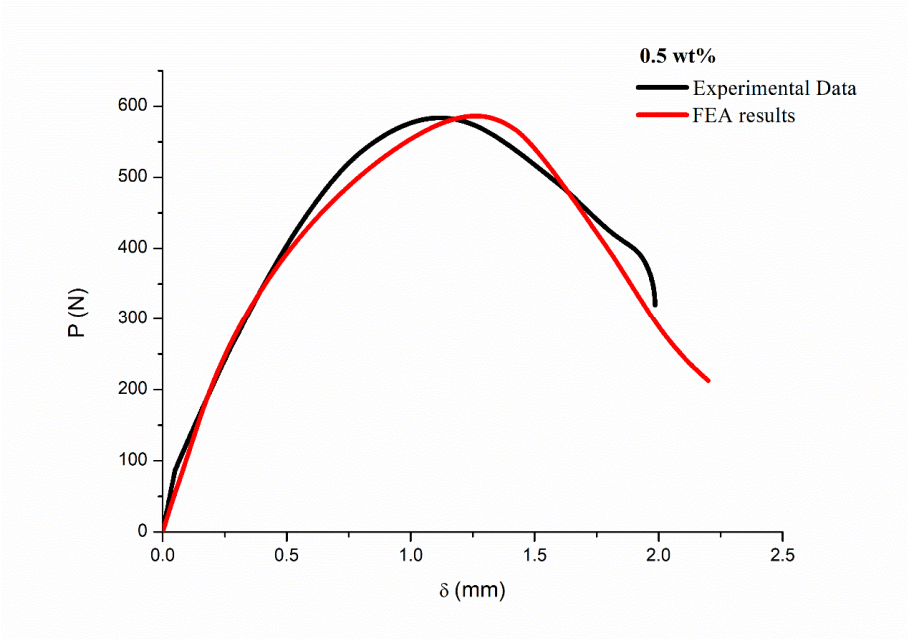

(c) 0.5 wt%

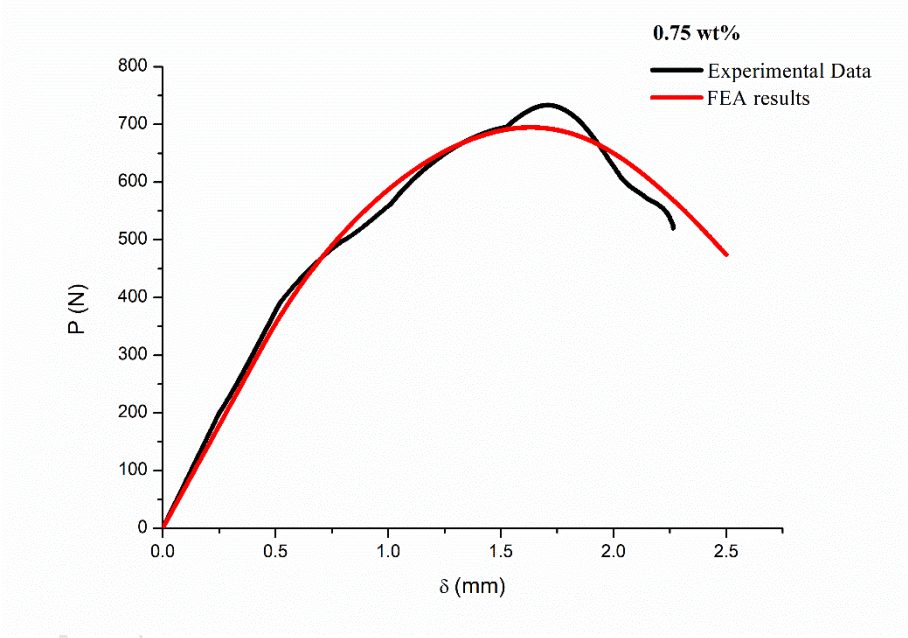

(d) 0.75 wt%

Fig.8. Comparison of the experimental and numerical results of DCB specimens with different GNP content of nanocomposites.

4 Conclusion

This paper conducted experiments on fracture resistance of the nanocomposites

with different graphene content by DCB specimens. The results show that mode I fracture toughness of nanocomposites increased compared the neat epoxy. The mode I fracture toughness of nanocomposites reinforced by 0.25 wt% graphene increased by 5 times compared with neat epoxy adhesive, which was the highest improvement among all the nanocomposites. With the graphene content continued to increase, the mode I fracture toughness of adhesive decreased as the aggregation of graphene in the epoxy adhesive. The mechanical behavior of the DCB specimens with different nanocomposites can be predicted by FEA with good consistency when CZM was used for different content of adhesive.

Acknowledgement

This Project is supported by the National Science Foundation for Young Scientists of China (Grant No. 51808261).

Reference

[1] Silva P, Valente T, Azenha M, Sena-Cruz J, Barros J. Viscoelastic response of an epoxy adhesive for construction since its early ages: Experiments and modelling. Compos Part B Eng 2017;116:266–77.

[2] Savvilotidou M, Vassilopoulos AP, Frigione M, Keller T. Effects of aging in dry environment on physical and mechanical properties of a cold-curing structural epoxy adhesive for bridge construction. Constr Build Mater 2017;140:552–61.

[3] Jia Z, Yuan G, Ma HL, Hui D, Lau KT. Tensile properties of a polymer-based adhesive at low temperature with different strain rates. Compos Part B Eng

2016;87:227–32.

[4] Wu Q, Li L, Zhang Y, Shui WJ. Absorption and mechanical properties of SiCp / PVDF composites. Compos Part B 2017;131:1–7.

[5] Wu Q, Si Y, Wu Y, Wang S, Wang G. Fabrication and absorption properties based on ZnO nanocomposites adjusted by length – diameter ratio of ZnO nanorods. Cryst Eng Comm 2016;18:4027–31.

[6] Jia Z, Hui D, Yuan G, Lair J, Lau K tak, Xu F. Mechanical properties of an epoxy-based adhesive under high strain rate loadings at low temperature environment. Compos Part B Eng 2016;105:132–7.

[7] Costa I, Barros J. Tensile creep of a structural epoxy adhesive: Experimental and analytical characterization. Int J Adhes Adhes 2015;59:115–24.

[8] Abouhamzeh M, Sinke J, Jansen KMB, Benedictus R. Kinetic and thermo-viscoelastic characterisation of the epoxy adhesive in GLARE. Compos Struct 2015;124:19–28.

[9] Bazilevs Y., Korobenko A., Deng X., Yan J. Fluid-Structure Interaction Modeling for Fatigue-Damage Prediction in Full-Scale Wind-Turbine Blades. J Appl Mech 2018; 83: 0610101–9.

[10] Deng X, Korobenko A, Yan J, Bazilevs Y. Isogeometric analysis of continuum damage in rotation-free composite shells. Comput Methods Appl Mech Engrg 2015;284:349–72.

[11] Bazilevs Y., Deng X., Korobenko A., Lanza di Scalea F., Todd MD, Taylor SG. Isogeometric Fatigue Damage Prediction in Large-Scale Composite Structures

Driven by Dynamic Sensor Data 2018;82: 0910081-12

[12] Wang Z, Liu X, Shen X, Han NM, Wu Y, Zheng Q, et al. An Ultralight Graphene Honeycomb Sandwich for Stretchable Light-Emitting Displays. Adv Funct Mater 2018.

[13] Sun T, Fan H, Wang Z, Liu X, Wu Z. Modified nano Fe_2O_3-epoxy composite with enhanced mechanical properties. Mater Des 2015;87:10–6. doi:10.1016/j.matdes.2015.07.177.

[14] Tee DI, Mariatti M, Azizan A, See CH, Chong KF. Effect of silane-based coupling agent on the properties of silver nanoparticles filled epoxy composites. Compos Sci Technol 2007;67:2584–91.

[15] Saba N, Safwan A, Sanyang ML, Mohammad F, Pervaiz M, Jawaid M, et al. Thermal and dynamic mechanical properties of cellulose nanofibers reinforced epoxy composites. Int J Biol Macromol 2017;102:822–8.

[16] Ravindran AR, Ladani RB, Wu S, Kinloch AJ, Wang CH, Mouritz AP. Multi-scale toughening of epoxy composites via electric field alignment of carbon nanofibres and short carbon fibres. Compos Sci Technol 2018;167:115–25.

[17] Mecklenburg M, Mizushima D, Ohtake N, Bauhofer W, Fiedler B, Schulte K. On the manufacturing and electrical and mechanical properties of ultra-high wt.% fraction aligned MWCNT and randomly oriented CNT epoxy composites. Carbon N Y 2015;91:275–90.

[18] Liew KM, Lei ZX, Zhang LW. Mechanical analysis of functionally graded

carbon nanotube reinforced composites: A review. Compos Struct 2015;120:90–7.

[19] Wang Z, Jia Z, Feng X, Zou Y. Graphene nanoplatelets/epoxy composites with excellent shear properties for construction adhesives. Compos Part B Eng 2018;152:311–315.

[20] Tang LC, Wan YJ, Yan D, Pei YB, Zhao L, Li YB, et al. The effect of graphene dispersion on the mechanical properties of graphene/epoxy composites. Carbon N Y 2013;60:16–27.

[21] Chandrasekaran S, Seidel C, Schulte K. Preparation and characterization of graphite nano-platelet (GNP)/epoxy nano-composite: Mechanical, electrical and thermal properties. Eur Polym J 2013;49:3878–88.

[22] Ekrem M, Avc A. Effects of polyvinyl alcohol nano fi ber mats on the adhesion strength and fracture toughness of epoxy adhesive joints 2018;138:256–64.

[23] Wang Z, Shen X, Han NM, Liu X, Wu Y, Ye W, et al. Ultralow Electrical Percolation in Graphene Aerogel/Epoxy Composites. Chem Mater 2016;28.

[24] Miculescu M, Thakur VK, Miculescu F, Voicu SI. Graphene-based polymer nanocomposite membranes: a review. Polym Adv Technol 2016;27:844–59.

[25] Anwar Z, Kausar A, Rafique I, Muhammad B. Advances in Epoxy/Graphene Nanoplatelet Composite with Enhanced Physical Properties: A Review. Polym - Plast Technol Eng 2016; 55:643–62.

[26] Wang Z, Shen X, Akbari Garakani M, Lin X, Wu Y, Liu X, et al. Graphene aerogel/epoxy composites with exceptional anisotropic structure and

properties. ACS Appl Mater Interfaces 2015;7:5538–49.

[27] Quan D, Carolan D, Rouge C, Murphy N, Ivankovic A. Mechanical and fracture properties of epoxy adhesives modified with graphene nanoplatelets and rubber particles. Int J Adhes Adhes 2018;81:21–9.

[28] de Moura MFSF, Goncalves JPM, Chousal JAG, et al. Cohesive and continuum mixed-mode damage models applied to the simulation of the mechanical behaviour of bonded joints. International Journal of Adhesion and Adhesives, 2008, 28: 419-426

[29] de Moura MFSF, Campilho RDSG, Goncalves JPM. Crack equivalent concept applied to the fracture characterization of bonded joints under pure mode I loading. Composites Science and Technology, 2008, 68: 2224-2230

[30] Campilho RDSG, Moura DC, Goncalves DJS, et al. Fracture toughness determination of adhesive and co-cured joints in natural fibre composites. Composites Part B-Engineering, 2013, 50: 120-126